CIV Polarization Measurements using a Vacuum Ultraviolet Fabry-Pérot Interferometer

Edward West1[1], G. Allen Gary[2], Jonathan Cirtain[1], John Davis[1]
Ken Kobayashi[2] and Chris Pietraszewski[3]
[1]Space Science Office, VP62, NASA Marshall Space Flight Center, Huntsville, AL 35812
[2]The University of Alabama, Huntsville, CSPAR, Huntsville, AL 35899
[3]IC Optical Systems Ltd, United Kingdom

ABSTRACT

Marshall Space Flight Center's (MSFC) is developing a Vacuum Ultraviolet (VUV) Fabry-Pérot Interferometer that will be launched on a sounding rocket for high throughput, high-cadence, extended field of view CIV (155nm) measurements. These measurements will provide (i) Dopplergrams for studies of waves, oscillations, explosive events, and mass motions through the transition region, and, (ii), polarization measurements to study the magnetic field in the transition region. This paper will describe the scientific goals of the instrument, a brief description of the optics and the polarization characteristics of the VUV Fabry Pérot.

Keywords: Fabry-Pérot Interferometer, VUV Fabry-Pérot , Vacuum Ultraviolet, Polarization, CIV measurement

1. INTRODUCTION

Spectral-polarimetric measurements of Zeeman sensitive emission lines in the solar transition region are needed to determine the magnetic fields in this very important region of the solar atmosphere. In this region the magnetic field dominates all other forces and provides the gateway from the photosphere to the corona. These important magnetic field measurements are difficult to make because the magnetically sensitive lines that occur in this region are in the far ultraviolet. Since the Zeeman splitting is proportional to wavelength, it is reduced by a factor of four form measurements in the optical and requires an instrument design that has high optical efficiency with high-spectral and polarization sensitivity.

The MSFC group has developed a grating spectropolarimeter as a sounding rocket payload (SUMI) to demonstrate that these Zeeman splitting can be made at these wavelengths[1]. The problem with this instrument is that it requires a narrow slit that must be scanned across the region of interest resulting in poor temporal resolution for events that are expected to change rapidly. An alternative approach is to use a Fabry-Pérot interferometer (FPI) rather than a grating to isolate the line. This approach provides a relatively large field-of-view (FOV) but the filter must be tuned across the spectral line. Because of the higher throughput and the abilitiy to rapidly scan across the line, we believe that this approach is both feasible and a better solution for monitoring rapid changes in the structure of the transition region magnetic field. Section 2 describes the importance of magnetic and Doppler measurements in the transition region (TR), and why the strong resonance CIV emission lines at 154.8 and 155.0 nm were selected for this mission. Section 3 describes the baseline design for this sounding rocket program which will use the telescope and polarimeter develop for SUMI and a high resolution CIV Fabry-Pérot interferometer that has already been developed[2,3,4]. Finally, Section 4 describes the polarization properties of our VUV Fabry-Pérot that uses MgF_2 windows. While other flouride windows can transmit CIV (LiF, BF and CaF_2), MgF_2 has the best mechanical and chemical properties for polishing windows to the flatness required by a VUV FPI. Unfortunately, MgF_2 is birefringent. Therefore the safest position for a MgF_2 CIV Fabry-Pérot is after the analyzer. This is the location of the FPI in our baseline design but we will also discuss the option to place the FPI in front of our analyzer and how it would affect the polarization measurements.

2. SCIENCE OBJECTIVES

The sounding rocket payload we are considering is based on imaging, double etalon Fabry-Pérot filter system. This system will make measurements of the dual CIV resonance emission lines at 154.82/155.08nm that are formed in the transition region (TR) (Figure 1) . These strong CIV emission lines are (i) associated with 10^5 °K plasma at an effective plane-parallel height of 2000 km, (ii) Zeeman sensitive with Landé-g values of 1.167/1.333, and (iii) have line widths of ~20-30pm (200-300mÅ). The characteristics and spectral purity of these lines provide important line diagnostics for analysis of the transition region.

The development of a narrow-band tunable spectral filter with a bandpass of 2-10 pm for the CIV TR emission lines is possible with our current technology. The filter system, combined with a high resolution polarimeter, will allow us to make precision measurements of the magnetic field in the transition region.

2.1. Transition Region Measurements

A CIV FPI will provide magnetic field, Doppler and intensity measurements in the solar transition region where the atmospheric structure and dynamics are no longer dominated by the gas pressure but are controlled by the magnetic field (Figure 1). By observing the triply ionized carbon atom (CIV) emission lines that are formed at a temperature of 10^5 °K in the upper transition region, the instrument is ideally suited for measuring the flow of magnetic and kinetic energy into the corona. In this location and over areas the size of active regions, the FPI will provide high-resolution, rapid-cadence magnetic field maps with a sensitivity of <50 G and velocity field maps with a sensitivity of <1 km s^{-1}. These observations will yield a new insight into the role of the release of the energy stored in the non-potential magnetic field in both steady state (coronal heating) and transient phenomena (solar flares and coronal mass ejections (CMEs)), two of the outstanding questions of solar physics.

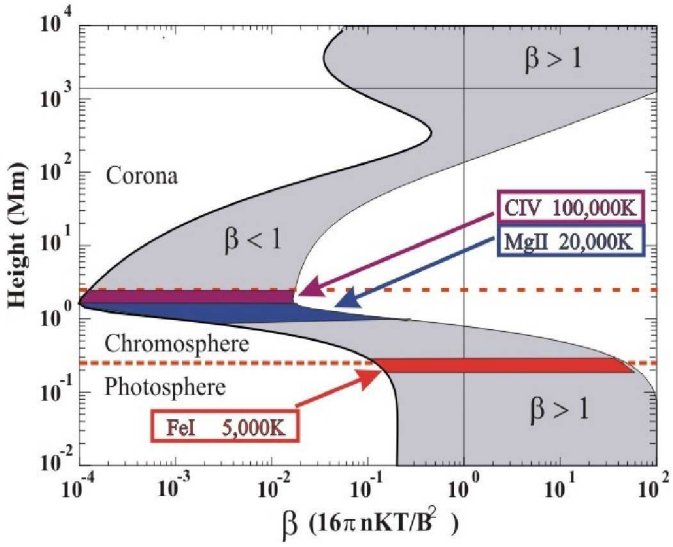

Figure 1. Plot illustrates the plasma pressure over an active region. The low beta (β) indicates that the CIV region responses most rapidly to magnetic field changes. Observing these rapid changes in both the Line Of Sight (LOS) magnetic field and the resulting plasma Doppler velocities are our ultimate science objectives (Gary 2001)[5].

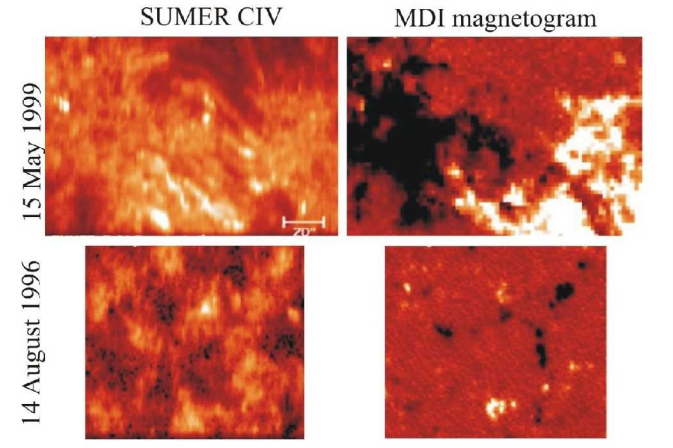

Figure 2. Comparison of SUMER CIV transition region images and MDI photospheric magnetograms.

Our science goal for this program is to understand the magnetically controlled transfer of non-thermal energy through the transition region to the corona. To achieve this broad goal, our instrument development program has the following major science objectives:

1. To understand how coronal heating is driven from below the corona.

2. To understand how the magnetic field stores and releases energy in the production of coronal mass ejections and flares.

Both objectives are inherently linked to line-of-sight (longitudinal) magnetic field maps of the β-minimum coronal base. Our CIV FPI's temporal resolution and magnetic and Doppler sensitivity will enable observation of (1) the motions, events, and magnetic conditions at the coronal base that are signatures of the drivers of coronal heating, and (2) the buildup, triggering, and release of the stressed magnetic fields at the low-β coronal base before and during major CME/flare eruptions.

The CIV emission lines are formed at the base of the corona. When one compares the SUMER CIV spectroheliograms to the MDI photospheric magnetograms, it is obvious that the CIV emission is generally brighter where the magnetic field is stronger in both active and quiet regions (Figure 2). In both regions, the CIV emission forms a patchy undulating "layer" that is a few thousand kilometers thick and is located ~2000 km above the photosphere. In quiet regions, this layer outlines the magnetic network and, at the limb, it forms a ragged "forest" ~5,000 km high[6]. In active regions (ARs), a small fraction of the CIV emission is in loops and plumes that extend into the corona.

A major challenge in modeling coronal heating is the large span of structural length scales, from the width of an AR down to the thickness of current sheets in braided flux tubes. New computational techniques and increasing computing power are allowing the development of quasi-realistic simulations of the transition region and corona. With solar observations from our CIV FPI, 3D models can be developed and parameters adjusted to fit our data together with those of space-based missions such as SDO and Hinode. With 3D models describing the solar atmosphere we hope to understand the process or processes through which the corona is heated.

3. OPTICAL DESIGN

Much of the technology that will be used in our CIV FPI sounding rocket program was develop for a previous sounding rocket program called SUMI, the Solar Ultraviolet Magnetograph Investigation. SUMI began as a set of technology development programs to improve the efficiency of polarization measurements in the ultraviolet. This section will describe the telescope and polarimeter that were developed for SUMI and the separate technology program though which the high resolution CIV FPI was developed. These three technology programs will be used in a future sounding rocket program (Solar Ultraviolet Filter Magnetograph - SUrF) that we plan to develop and will be described in the next three sections.

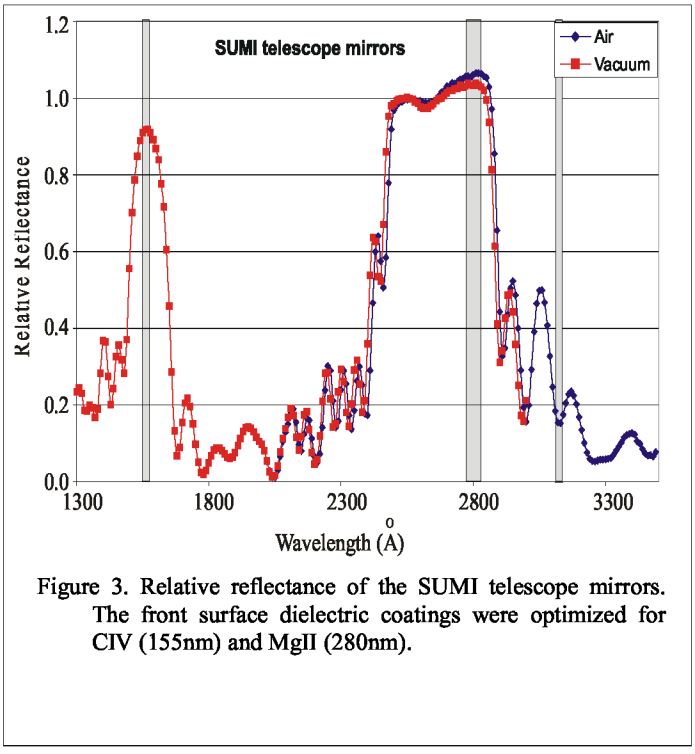

Figure 3. Relative reflectance of the SUMI telescope mirrors. The front surface dielectric coatings were optimized for CIV (155nm) and MgII (280nm).

3.1. SUMI Telescope

A solar telescope design must solve the thermal problems associated with direct solar viewing. The simplest solution is a Gregorian telescope with a field stop between the primary and secondary mirrors.

While this reduces the thermal load on the secondary, the disadvantages to this approach are a limited field of view, a longer optical path, and a larger secondary for on-axis designs, which decreases the effective collecting area of the telescope. The SUMI approach for decreasing the thermal load on the secondary mirror is to use a Ritchey-Chretien telescope with special dielectric coatings applied to the front surfaces of both the primary and secondary mirrors. These coatings reflect only narrow wavelength bands that contain the CIV and MgII emission lines at 155nm and 280nm. This results in a "cold mirror" or "self-filtering" telescope. The rear surface of the primary mirror has a parabolic figure and is coated with aluminum that reflects the unwanted solar radiation back into space. The advantages of this design are that the field of view is not restricted by a Gregorian stop (i.e. the whole Sun can be imaged) and, for a given instrument length, the shorter telescope allows a larger spectrograph which was important in improving SUMI's wavelength resolution. The narrowband UV reflection coatings simplify the thermal environment, minimize the infrared and visible light contamination of the spectral data, and act as a blocking filter for the spectrograph. The measured reflectance of these coatings is shown in Figure 3.

The reflectance of the two wavelength bands is achieved by placing a fluoride pi stack[7,8] that reflects the CIV wavelengths on top of an oxide stack that reflects the MgII wavelength band. In this coating design the MgII band was adjusted to minimize the contamination of the 310nm reflectance into SUMI's CIV 2nd order measurement. The preferred approach is to build a second set of mirrors with only the CIV flouride coating. This would eliminate the additional CIV fold mirrors required to act as the prefilter for the CIV FPI (section 3.3). While this is the ideal solution, the actual decision will be based on a cost versus optical efficiency study.

3.2. SUMI Polarimeter

The polarimeter follows the telescope and consists of a rotating waveplate and a double Wollaston analyzer. Due to the low photon flux at CIV and the weak linear polarization levels, the waveplate was designed to measure circular polarization at CIV (270° retardance at 155nm)[10,11]. Exploratory linear measurements [Q] could be made when the fast axis of the waveplate is aligned parallel to the transmission axis of the analyzer.

The double Wollaston analyzer, which is a polarizing beamsplitter, is the most efficient UV polarizer in this wavelength band[11]. Figure 4 shows the orientation of the double Wollaston and the exiting linearly polarized beams (½(I±Q)). The orientation of the linear polarization and how it interacts with the CIV VUV FPI is described in Section 4.2.

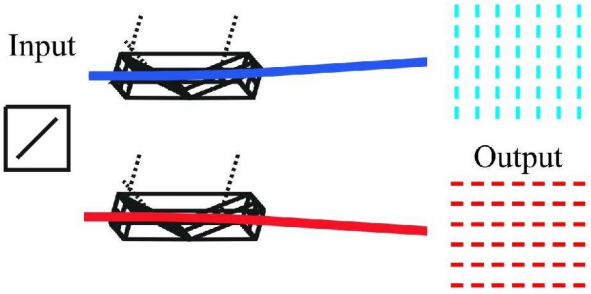

Figure 4. SUMI double Wollaston Analyzer. The vertical polarization (**blue**) is defined to be ½(I+Q), the horizontal polarization (**red**) ½(I-Q).

Because the CIV emission is very dynamic, a dual-beam analyzer is very important for transition region magnetic field measurements. Without simultaneous measurements of orthogonal polarizations, intensity crosstalk can create false signals in the magnetic field measurements. Since both polarizations are observed simultaneously, the total transmission is much higher than traditional reflective polarizers that is particularly important at CIV. Finally, the polarization resolution ($<10^{-3}$) is higher and covers a larger wavelength range than traditional reflective analyzers.

Since the SUMI double Wollaston design was set by the MgII beam separation, one option that is being considered is to redesign the double Wollaston with a smaller CIV beam separation. Reducing the beam separation has several advantages in the optical design of SUrF. The first advantage is to reduce the angle of incidence on the CIV FPI . This will be discussed in both section §3.4 and in the section describing the polarization modeling of the CIV FPI (§4.1). The second advantage is to reduce the aberrations created by the double Wollaston. Unlike SUMI, SUrF is a single wavelength experiment (155nm) and chromatic aberrations are not important but the birefringence and thickness of the MgF_2 double Wollaston can produce astigmatism.

3.3. CIV Fabry Pérot Interferometer

Gary et al. (2007)[2] described the details of the CIV FPI instrument development program that resulted in a tunable VUV FPI. This program accomplished the following goals: Two pairs of MgF_2 etalon plates were polished to better than a $\lambda/150$ at 633 nm or $\lambda/24$ at 155 nm (with a plate finesse of $F_D > 12$). A primary set of test plates were coated with a 77% relative reflectance at 155 nm. The coatings were VUV dielectric coatings having low-absorption pi-coatings. This set of MgF_2 plates were then overcoated with a silver coating to determine if any stress from the pi-coating would reduce the plate finesse. The pi-coating was then applied to the second pair of etalon plates and this set of MgF_2 plates was assembled into the high resolution FPI (HRI). The plates were mounted into a piezoelectric-tunable, capacitance-stabilized etalon with a Hovemere's Hansen split-spring optical mount for low induced mechanical stress. The primary set of test plates will be used to develop our Low Resolution Interferometer (LRI, Figure 5). Figure 7 shows the etalon scans made with an F_2 laser whose dominant emission line is 157.63 nm. The data show the results from the development program of the pi-coatings, the polishing of the magnesium fluoride plates, and the assembly of the etalons within a Hanson split-spring mount. The result was an operational and robust CIV VUV interferometer (Figure 6) that provides confidence that a total finesse of greater than 15 is an achievable goal. With the carbon arc lamp recently developed to support SUMI, we will be able to scan the FPI through the CIV emission lines. The design, fabrication, and operation of multi-etalon interferometers have been given in a number of papers[12,13,14].

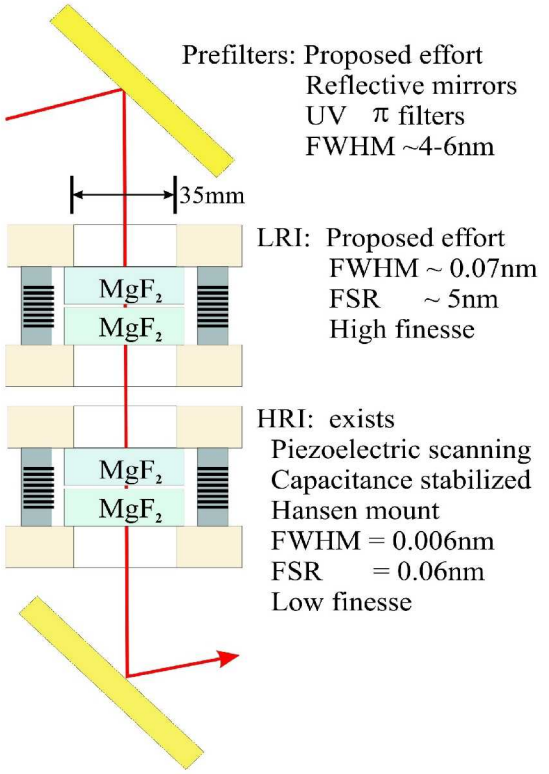

Figure 5. Optical sketch of dual CIV Fabry Pérot filter system.

Figure 6. High resolution CIV Fabry Pérot Interferometer (Gary 2007)[2].

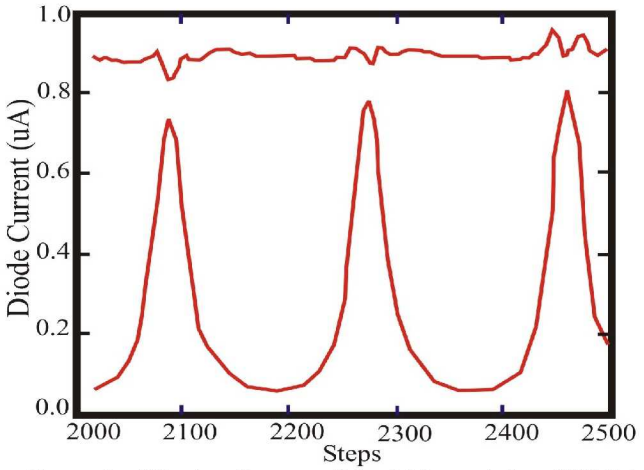

Figure 7. Wavelength scan of the high resolution CIV Fabry Pérot Interferometer shown in Figure 6 (Gary 2007)[2].

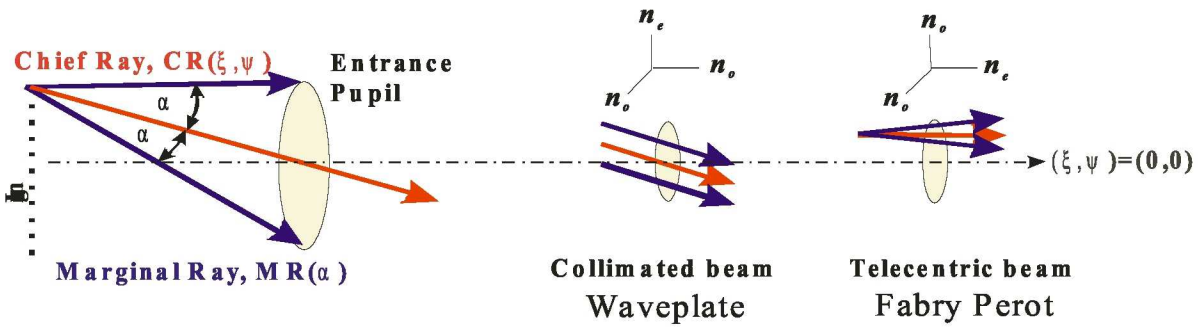

Figure 8. Optical definitions showing the orientation of the indices of refraction for a MgF_2 waveplate and Fabry Pérot. The n_e (the extra-ordinary index of refraction, n_o is the ordinary index) axis is the optic axis of a birefringent uniaxial crystal; the optical axis of the instrument is the (ξ,ψ)=(0,0) direction. In a collimated beam the marginal rays and chief rays from each point in the image plane are parallel; in a telecentric beam every chief ray in the image plane is parallel.

3.4. SUrF optical design

Figure 9 compares the optical design of SUMI with that being developed for our SUrF sounding rocket program. Placing the FPIs in front of the analyzer would make a more compact instrument but the FPI etalons are made with MgF_2. While MgF_2 transmits to 115nm, it is birefringent. Therefore, the alignment of the optic axis (*ne*, see Figure 8) of four MgF_2 FPI plates will require greater precision and would significantly increase the cost for a CIV FPI in front of the analyzer (position B in Figure 9). Therefore, our default design is to place the CIV FPI after the analyzer (position A in Figure 9). In this position any "retardance" of the filter would not affect the polarization measurements made by the rotating waveplate. While there could be an instrumental polarization bias created by the linear polarization exiting the double Wollaston analyzer and the folding mirrors, the CIV FPI in this position and in a collimated beam would produce a large instrumental polarization pattern that could easily be corrected over the field of view of the SUrF camera system.

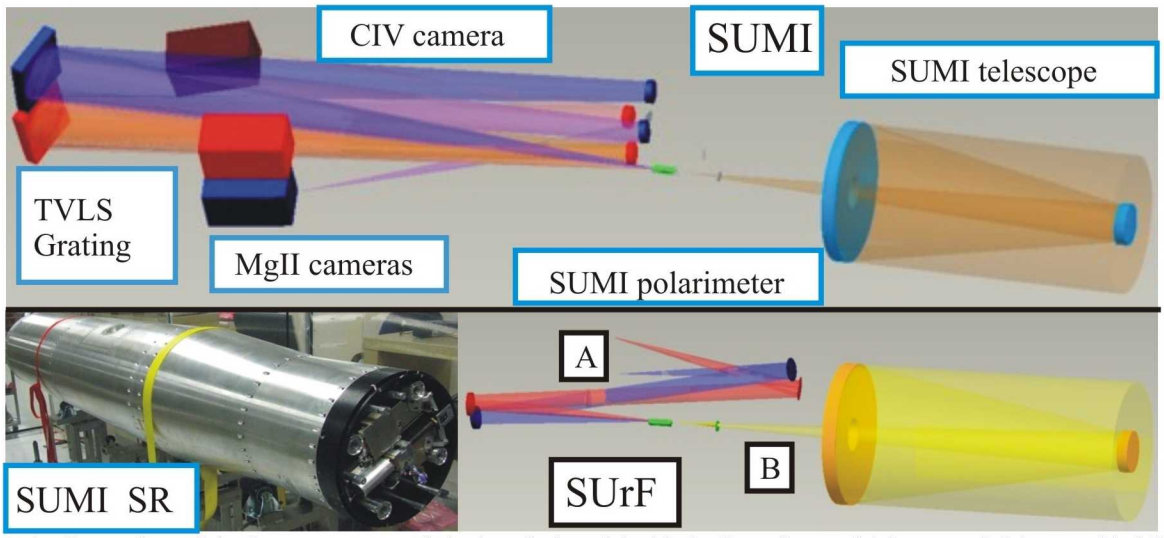

Figure 9. Comparison of the SUMI spectrograph (top) optical model with the SUrF (lower right). Lower left is assembled SUMI sounding rocket ready for delivery to White Sands Missile Range. SUrF will use SUMI's telescope, polarimeter, the MgII cameras and the CIV data system.

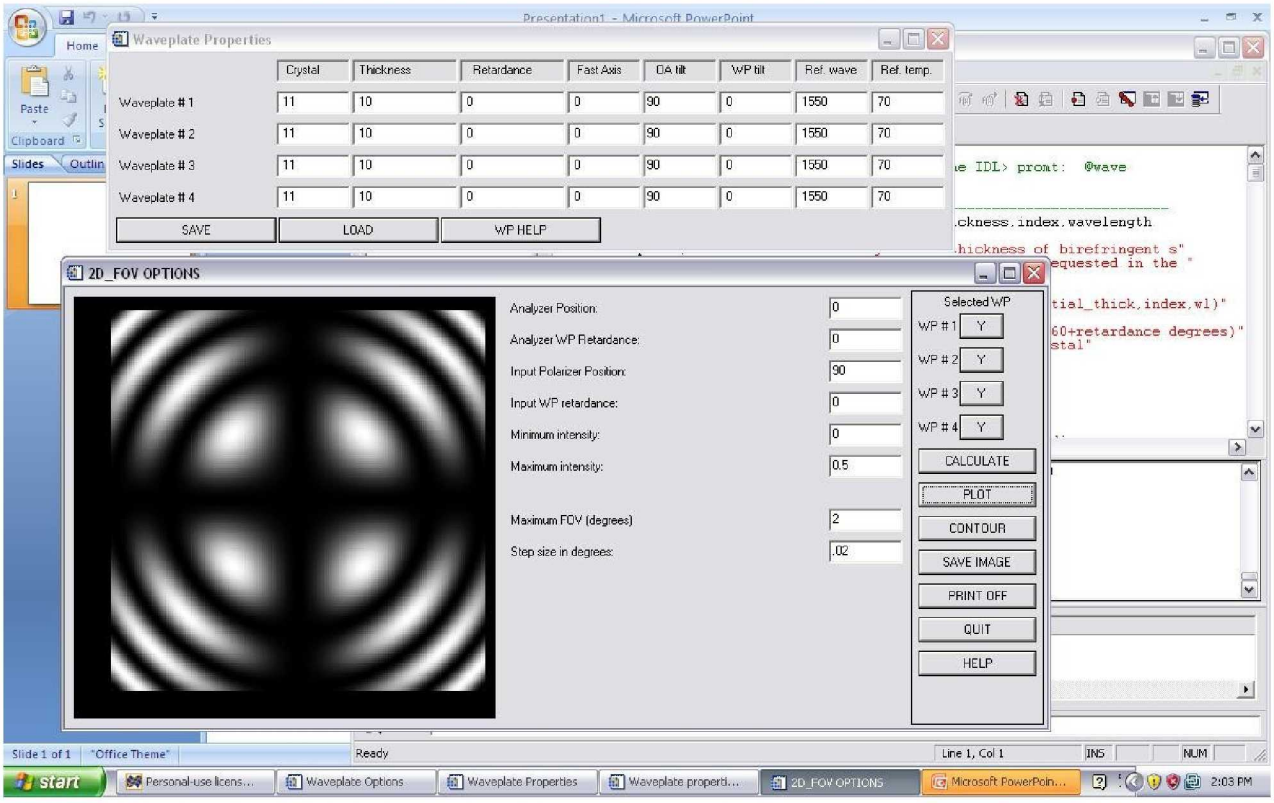

Figure 10. Screenshot of a polarization program developed to model the field of view characteristics of birefringent optics. This model shows the setup for the SUrF CIV FPI that will be described in Section 4.1. The thickness of the four MgF_2 windows that make up the LRI and HRI is 10mm each and the windows are placed between crossed linear polarizers (Input polarizer at 90 and analyzer at 0 degrees). To model the CIV FPI between between crossed circular polarizers, a 90 degree retardance is placed in the Analyzer and Input waveplate rows.

If the CIV FPI was placed in a telecentric beam, variations in the birefrigence of the four MgF_2 etalon plates would have to be corrected. Field of view (FOV) and birefringent errors will be discussed in greater detail in the next section.

4. POLARIZATION PROPERTIES OF THE CIV FPI

The main goal in the development of the CIV FPI was to prove that a tunable, narrowband FPI was possible in the vacuum ultraviolet (VUV). With the successful completion of that program and after several flights of SUMI, there is an option to add the CIV FPI to the optical path of the SUMI slitjaw camera. Certainly this would require restructuring the SUMI payload to reduce the mass and power; probably eliminating the MgII measurements and having an all CIV mission. With that option the CIV FPI would simply make narrowband CIV intensity and dopplergrams which was the original intent in the VUV FPI development program. With SUrF magnetic field measurements have been added. Therefore, the polarization properties of the CIV FPI are important in selecting the optimum position in the SUrF optical design. The next section (§4.1) will describe the requirements of a CIV FPI making polarization measurements at position B in Figure 9. Section 4.2 will show the polarization patterns of various MgF_2 plates including the CIV FPI.

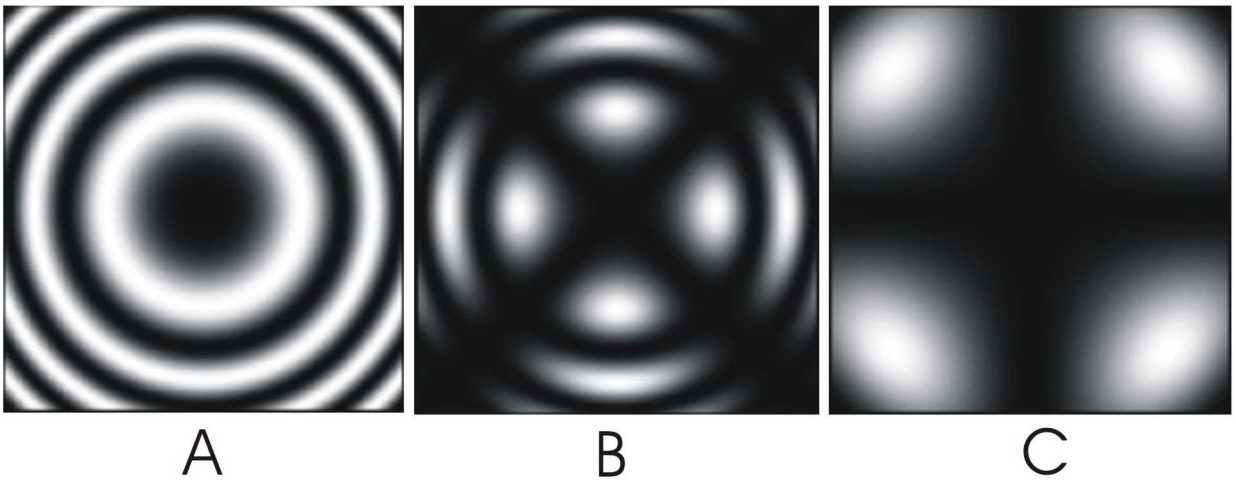

Figure 11. Polarization model of the patterns that should be seen in an ideal CIV FPI. (A) is the same optical design as Figure 10 except between crossed circular polarizers. This is the best way to show how the retardance varies with the angle of incidence. (B) is the same as Figure 10 except with the input and exit polarizers rotated by 45 degrees. (C.) is the FOV of only one of the four 10mm MgF_2 windows.

4.1. Polarization model

Figure 10 shows the polarization model of an ideal CIV FPI including the MgF_2 plates for both the HRI and the LRI (Figure 5). The thickness of the two MgF_2 etalon plates in Figure 6 is 10mm. When the CIV HRI was ordered, the material, reflectivity, free spectral range and finesse were specified; other than ordering MgF_2 windows, the orientation of the optic axis (ne) was not specified. In this model, the orientation of the optic axis is assumed to be perpendicular to the polished surface. This of course is the ideal orientation for any birefringent crystal and produces a zero retardance along the optic axis. In Figure 10 the four MgF_2 plates are placed between linear polarizers which form a cross. That cross outlines the orientation of the fast and slow axes of the plates and the transmission axes of the linear polarizers and the rings reflect the off-axis retardance. To view only the retardance variation, the MgF_2 plates can be placed between crossed circular polarizers (Figure 11.A). If the plates are perfectly polished, rotating any of the plates will not change the polarization patterns seen in Figures 10 and 11. Two MgF_2 plates (white and blue outlines in Figure 12) were ordered with the requirement that the optic axis be within 5 arc minutes of the polished surface and meet this polarization requirement. A third MgF_2 (red circle in Figure 12), which was used to correct field of view errors in a two

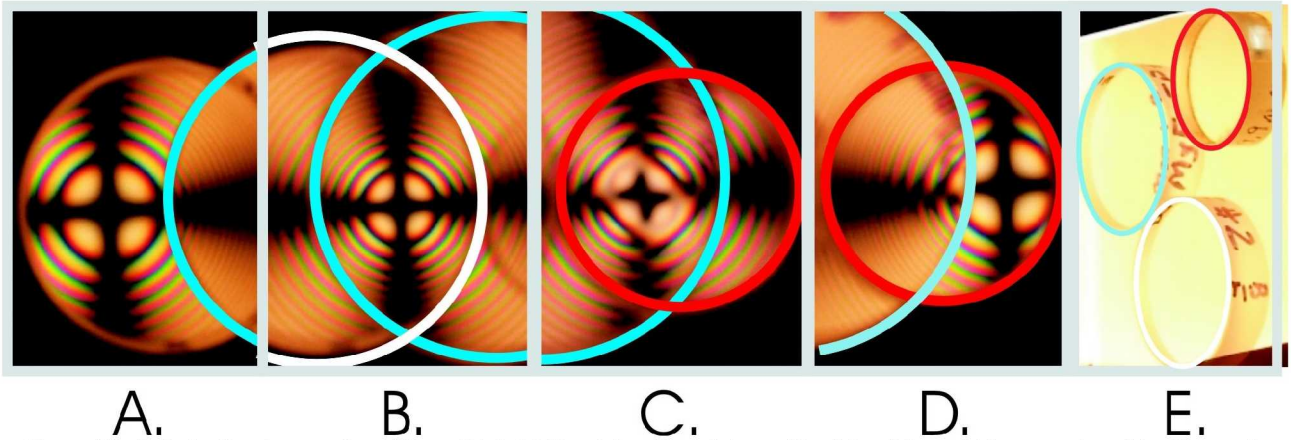

Figure 12. Polarization images from 10mm thick MgF_2 plates. The plates outlined in white and blue were bought with a optic axis error of less than 5 arc minute from the normal to the polished surface. The MgF_2 plate in red was bought to support a two KD*P polarimeter and has an optic axis error less than 1 degree[15].

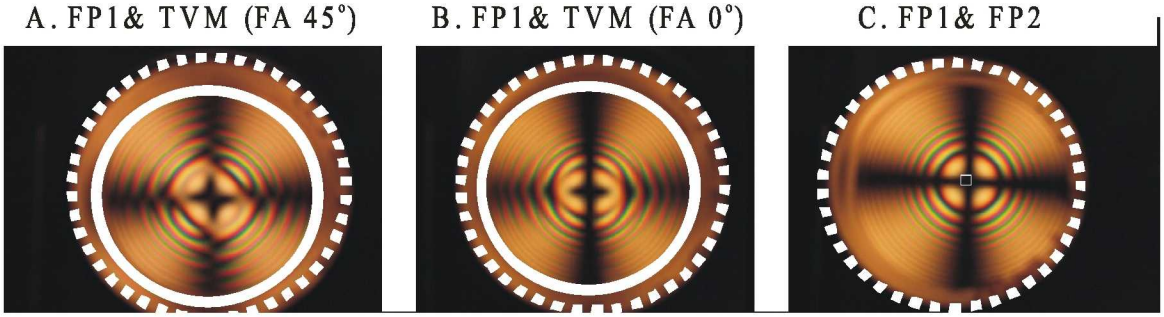

Figure 13. MgF_2 windows between crossed linear polarizers. All of the MgF_2 windows (optic axis toward observer) are 10mm thick. Two MgF_2 windows (FP1 and FP2 in C.) were purchase with a requirement that the optic axis (n_e) by align to within 5′ of the polished surface. Rotating the two MgF_2 plates in Figure C produces no separation in the cross pattern → therefore, no retardance. The TVM MgF_2 waveplate was use to correct FOV errors in the Tower Vector Magnetograph (TVM) KD*P polarimeter15 (West, 1978). The COBRA MgF_2 plates (FP1 & FP2) are 40mm diameter plates (dash lines) while the TVM MgF_2 plate (solid line) is 25mm. Because of the optic axis error in the TVM MgF_2 plate there is a retardance error in Figure A (separation of cross pattern). In Figure B, the retardance error in the circular polarization measurement is minimize by rotating the "FA" of the TVM MgF_2 parallel to the transmission axis of the linear analyzer.

KD*P polarimeter[15], was specified to have the optic axis within 1 degree. As it is rotated on top of one of the 5arc minute MgF_2 plates, the cross can be seen to separate which indicates that it is acting as a retarder (Figure 13.A). The only option for using this pair of MgF_2 plates in position B of Figure 9 would be to align them so that their "apparent" fast and slow axes are aligned to the transmission axis of the double Wollaston analyzer (Figure 13.B).

4.2. Polarization measurements

Measurements by the vendor on the backup set of MgF_2 windows which may be used in the LRI (Figure 5) indicate that the optic axis of those plates is ~9.5 degrees from the polished surface. Unfortunately, viewing the polarization pattern through the CIV FPI with such a large optic axis angle is difficult. Figure 14 shows the on-axis (A) and the far field (B) polarization patterns. The MgF_2 plates in Figure 15 have a similar optic axis error as the CIV FPI but the FOV is not restricted by the mechanical package. From Figure 15, the polarization patterns suggest that the optic axes of the MgF_2 plates in the HRI (Figure 6) are almost 180 degrees apart. Certainly this is the worst configuration and requires that the CIV FPI be placed after the double Wollaston analyzer.

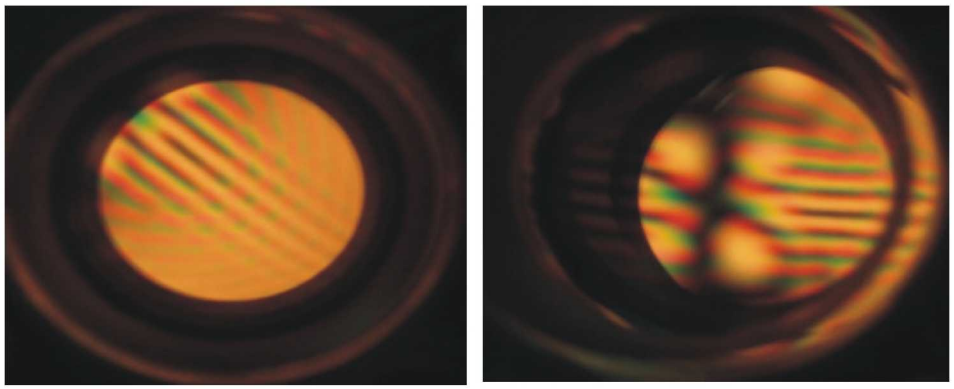

Figure 14. CIV FPI between crossed linear polarizers. Picture (A.) is perpendicular to the MgF_2 windows and (B.) nearly 15 degrees. The field of view is restricted by the mechanical packaging but (B.) is similar to the image (C.) in Figure 15.

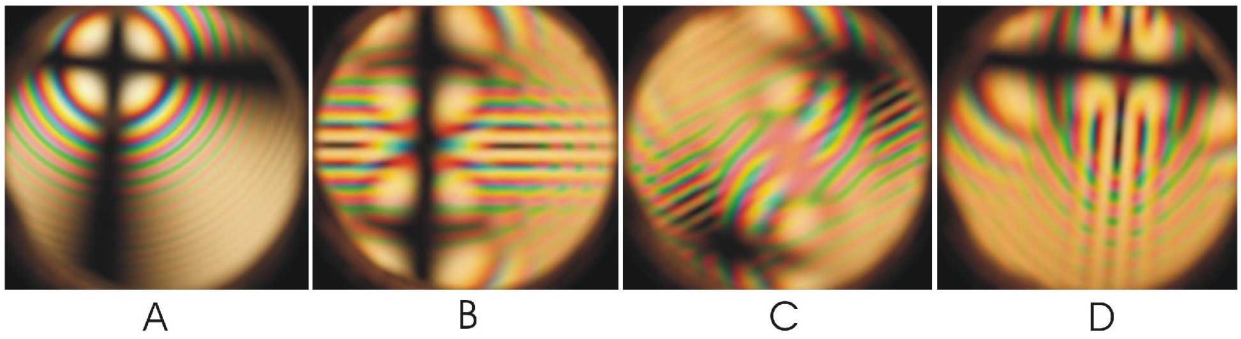

Figure 15. MgF_2 windows used to protect the CIV FPI. The thickness of these windows is 6mm and the optic axis angle ~8 degrees from polished surface. (A.) both MgF_2 windows co-aligned between crossed polarizers, (B.) the top MgF_2 rotated ~90 degrees, (C.) ~180 degrees and (D.) 270 degrees.

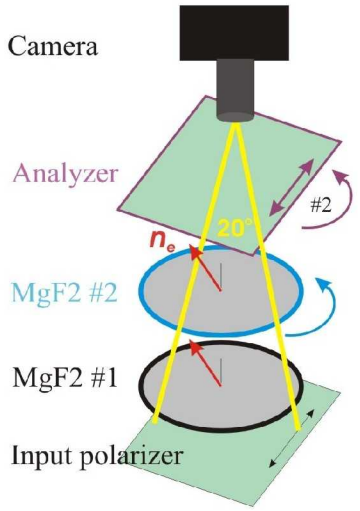

Figure 16. Test setup for MgF_2 images in Figure 15. In those images only the top MgF_2 plate (#2) is rotated.

5. SUMMARY

While our CIV FPI program has been built around using exiting hardware, there are two areas that could significantly improve the performance of our polarization measurements: (1) the development of a telescope that reflects only the CIV line and (2) replacing the MgF_2 etalon plates with plates where the optic axis is within 5 arc minutes of the normal to the polished surface. This would greatly improve the polarization measurements, the thermal environment and allow us to significantly reduce the payload mass.

6. REFERENCES

[1] E. A. West, K. Kobayashi, J. M. Davis and G. A. Gary, "The Solar Ultraviolet Magnetograph Investigation Sounding Rocket Program," SPIE: Solar Physics and Space Weather Instrumentation II, **6689**, 1-12 (2007).

[2] Gary, G. A., West. E. A., Rees, D., McKary, J., Zukic, M., and Herman, P., "Solar CIV Vacuum Ultraviolet Fabry-Perot Interferometer for Solar Research," *Astronomy and Astrophysics*, **461**, 707 (2007).

[3] Gary, G. A., West, E. A., Rees, D.,, Zukic, M., Herman. P., & Li, J., "CIV Vacuum Ultraviolet Fabry-Perot Interferometers for the Transition Region Magnetography", ASP Conf., **358**, 181 (2006).

[4] Gary, G. A., Davis, J. D., & West, E. A., "Future Possibilities for Doppler and Magnetic Field Measurements in the Extended Solar Atmosphere: Dissecting the Transition Region", Advances in Space Research, **43**, 96 (2009).

[5] Gary, G. A, "Plasma Beta above a Solar Active Region: Rethinking the Paradigm," *Solar Phys.*, **203**, 71-86 (2001).

[6] Mariska , J. T., [The Solar Transition Region], Cambridge: Cambridge University Press, (1992).

[7] Zukic, M., & Toor, D. G., [Thin Films for Optical Coatings], eds., R. E. Hummel & K. H.. Guenther, New York: CRC Press, 79 (1995).

[8] Zukic, M., Torr, D. G., Spann, J. F., and Torr, M. R., *Opt. Eng.*, **32**, 3029 (1993).

[9] West, E. A., J. G. Porter, J. M. Davis, G. A. Gary, M. Adams, S. Smith and J. F. Hraba, "Optical characteristics of the Marshall Space Flight Center Solar Ultraviolet Magnetograph," SPIE: UV/EUV and Visible Space Instrumentation for Astronmy and Solar Physics, **4498**, 101-110 (2001).

[10] K. Kobayashi, E. A. West and M. Noble, "Polarization measurements in the Vacuum Ultraviolet," SPIE: Polarization Science and Remote Sensing II, **5888**, 1-12 (2005).

[11] West, E. A., J. G. Porter, J. M. Davis, G. A. Gary, and M. Adams, "Development of a polarimeter for magnetic field measurements in the ultraviolet," SPIE: Polarization Analysis: Measurement and Remote Sensing IV, **4481**, pp. 109-117 (2001).

[12] Gary, G. A., Balasubramaniam, K. S., and Sigwarth, M., "Multiple Etalon Systems for the Advanced Technology Solar Telescope", Innovative Telescopes and Instruments for Solar Physics , **4853**, 252-272 (2003).

[13] Kentischer, T. J., Schmidt, W., Sigwarth, M., and Uexkull M. V., "TESOS, a double Fabry-Perot instrument for solar spectroscopy -Perot filtergraphs," *A&A,* **447**, 1111 (1998).

[14] Tritschler, A, Schmidt, W., Langhans, W., Langhans, K, and Kentischer, T, "High-resolution solar spectroscopy with TESOS - Upgrade from a double to a triple system," *Solar Phys*, **211**, 17 (2002).

[15] E. A. West, "Extending the Field of View of KD*P Electro-Optic Modulators," *Applied Optics*, **17**, no. 18, 3010-3013 (1978).

[16] West, E. A., Gary, G. A., Noble, M., Choudhary, D. and Robinson,R., 2005, "Large Field-of-View KD*P Modulator for Solar Polarization Measurements," SPIE: Polarization Science and Remote Sensing II , **5888**, 1-12 (2005).